

Is CHF triggered by the vapor recoil effect?

Vadim Nikolayev, D. Beysens, D. Chatain

▶ **To cite this version:**

Vadim Nikolayev, D. Beysens, D. Chatain. Is CHF triggered by the vapor recoil effect?. 6th Int. Conf. on Boiling Heat Transfer, 2006, Spoleto, Italy. pp.1. hal-00163389

HAL Id: hal-00163389
https://hal.science/hal-00163389

Submitted on 17 Jul 2007

HAL is a multi-disciplinary open access archive for the deposit and dissemination of scientific research documents, whether they are published or not. The documents may come from teaching and research institutions in France or abroad, or from public or private research centers.

L'archive ouverte pluridisciplinaire **HAL**, est destinée au dépôt et à la diffusion de documents scientifiques de niveau recherche, publiés ou non, émanant des établissements d'enseignement et de recherche français ou étrangers, des laboratoires publics ou privés.

ECI International Conference on Boiling Heat Transfer
Spoleto, 7-12 May 2006

IS CHF TRIGGERED BY THE VAPOR RECOIL EFFECT?

V. S. Nikolayev[1,2]*, D. Chatain[1], D. Beysens[1,2]

[1]ESEME, Service des Basses Températures, DRFMC/DSM/CEA-Grenoble, 17 rue des Martyrs, 38054 Grenoble Cedex 9, France
[2]CEA-ESEME, ESPCI-PMMH, 10, rue Vauquelin, 75231 Paris Cedex 5, France

ABSTRACT

This paper deals with the triggering mechanism of the boiling crisis, a transition from nucleate to film boiling. We observe the boiling crisis in pool saturated boiling experimentally at nearly critical pressure to take advantage of the slowness of the bubble growth and of the smallness of the Critical Heat Flux (CHF) that defines the transition point. Such experiments require the reduced gravity conditions. Close to the CHF, the slow growth of the individual dry spots and their subsequent fusion on the transparent heater are observed through the latter. As discussed in the paper, these observations are consistent with numerical results obtained with the vapor recoil model of the boiling crisis.

hal-00163389, version 1 - 17 Jul 2007

INTRODUCTION

The boiling crisis, called also the "Departure from Nucleate Boiling" (DNB), is a transition from nucleate to film boiling. It is highly important for industrial applications of high heat flux boiling because of the rapid heat transfer decline at the moment of transition. A severe damage of the heater can result because of its overheating. DNB occurs at a threshold value of the heat flux, the Critical Heat Flux (CHF). Because of its importance, a large number of the CHF studies is being published each year since the first model suggested by Zuber [1]. While Zuber's CHF expression describes relatively well a number of experimental CHF data, the underlying physical model (vapor stems) does not correspond to most modern observations of DNB. Multiple semi-empirical correlations were proposed since that. However, the validity range for each corresponds basically to the range where the empirical constants were fitted. The predictive power of such correlations remains thus very limited.

All existing modern ideas (see e.g. [10] for their review) concerning the DNB triggering can be placed into two large classes. The first considers the heater drying is initiated by the growth of a single bubble as the primary mechanism. The second argues that the bubble crowding close to the heater leads to the fusion of multiple small dry spots. This paper develops an approach of the first type based on the vapor recoil concept proposed originally in [3]. The numerical simulations are performed. We discuss also recent experimental observations which corroborate this idea.

For the reasons of industrial importance, boiling is mostly studied at low pressures comparing to the critical pressure p_c (the pressure of the gas-liquid critical point) of the fluid under study, e.g. for water or freon at atmospheric pressure. CHF is then large (of the order of several MW/m^2 for water) and the boiling close to it is indeed extremely violent. However, it is well known that CHF decreases at high pressures where DNB can thus be observed at a smaller heat flux. In addition, the thermal diffusivity is smaller in this regime, the bubble growth slows down, and the optical distortions disappear due to the slowness of the fluid motion. From the point of view of the modelling, this slowness permits to simplify the problem by neglecting the hydrodynamic stresses at the bubble interface, the shape of which can then be calculated in the quasi-static approximation.

VAPOR RECOIL EFFECT ON THE BUBBLE SPREADING

Every fluid molecule evaporated from the liquid interface causes a recoil force analogous to that created by the gas emitted by a rocket engine. It pushes the interface towards the liquid side in the normal direction. The vapor recoil force appears because the fluid necessarily expands while transforming from liquid to gas phase. Obviously, the stronger the evaporation rate η (mass per time and interface area), the larger the vapor recoil force. The vapor recoil force per unit interface area is $P_r = \eta^2(\rho_V^{-1} - \rho_L^{-1})$, where $\rho_L(\rho_V)$ signifies liquid (vapor) density.

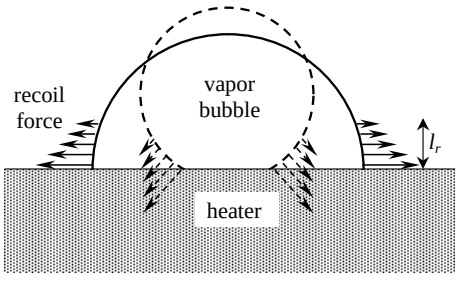


Figure 1. Sketch illustrating the vapor recoil effect. The amplitude and direction of the vapor recoil force are shown by arrows. The thickness l_r of the belt on the bubble surface, in which the vapor recoil force is important, is exaggerated with respect to the bubble size.

Let us now consider a growing vapor bubble attached to the heater surface (Fig. 1). While the temperature of the vapor-liquid interface is constant and equal to the saturation temperature for the given system pressure p for the pure fluid case (see

*e-mail: vadim.nikolayev@cea.fr

the discussion in [4–6] and references therein), a strong temperature gradient forms in the liquid near the heating surface. The liquid is overheated in a thermal boundary layer, and the heat flux q_L at the bubble surface is thus elevated in a "belt" of the bubble surface adjacent to the bubble foot. As a matter of fact, most of the evaporation into the vapor bubble is produced in this belt, whose thickness l_r is much smaller than the bubble radius. Since $\eta = q_L/H$, where H is the latent heat, the vapor recoil near the contact line is much larger than at the other part of the bubble surface and the contact line is pulled apart from the bubble center as if the contact angle increased. However the actual contact angle θ_{eq} depends only on the molecular forces and remains constant. The bubble curvature should thus increase near the contact line, see Fig. 2.

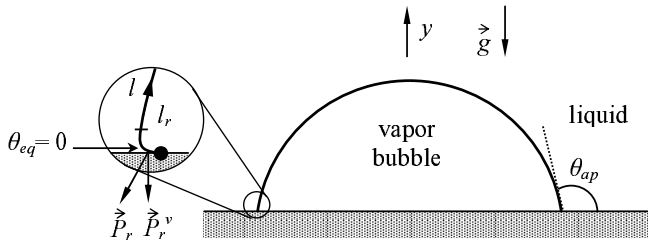


Figure 2. Apparent (θ_{ap}) and actual (θ_{eq}) contact angles. The vicinity of the contact line (zero for the curvilinear coordinate l measured along the bubble contour) is zoomed in. The arrows show the directions of the vapor recoil force and its vertical component responsible for an additional adhesion of the bubble to the heater.

In other words, the vapor recoil tends to extend the dry spot under the vapor bubble so that the bubble tends to cover the heater surface. However other forces acting on the bubble surface can counterbalance the vapor recoil. E. g. for the usual evaporation conditions, the vapor recoil is negligibly small with respect to the surface tension σ. Their relative magnitude is characterized by the ratio

$$N = \int P_r(l)\mathrm{d}l/\sigma, \tag{1}$$

where the integration is performed along the bubble contour, see Fig. 2 for the l definition. The spreading occurs when N becomes comparable with unity which corresponds to the heat flux from the heater of the order 1 MW/m^2 [3] for water at high pressure, i.e. to the flux comparable to the actual CHF. The spreading of a bubble is followed by the coalescence with its neighbors.

The effect of the vapor recoil is not limited to the bubble spreading. The vapor recoil creates an additional bubble adhesion to the heater that prevents the bubble departure as soon as the bubble spreading begins, i.e. when the vapor recoil becomes important [8]. This adhesion force can be obtained by integrating the vertical component P_r^v of $\vec{P}_r$ (Fig. 2) over the bubble interface. This point is extremely important because the CHF should be determined as a threshold between the bubble departure and spreading regimes. If the time of bubble residence on the heater is small, the bubble might simply do not have enough time to spread.

These considerations would not allow a CHF correlation to be obtained analytically. Thus the numerical simulations are necessary.

NUMERICAL MODELLING

The account of the vapor recoil effect requires the simulation of the bubble growth with a truly free surface. This complicates the simulation a lot. However, there is a one more problem associated with a singular (or quasi-singular) behavior of the local heat fluxes in the vicinity of the contact line. Indeed, since the thermal conductivity of the heater is usually much larger than that of the liquid, the heater is assumed isothermal at a temperature higher than the saturation temperature T_{sat} for the given system pressure. If the bubble surface is assumed isothermal at T_{sat} in agreement with the experimental and theoretical considerations [4–6], the resulting temperature ambiguity at the contact line leads to the non-integrable divergence, $q_L(l) \sim l^{-1}$. This shows importance of the thermal properties of the heater that need to be taken into account by solving the conjugate problem at least in liquid and solid domains.

Problem statement and its solution

At high pressures we can assume that the bubble growth is slow and than the viscous stresses at the bubble interface and the inertial expansion forces are much smaller than the surface tension. In this case the bubble shape is independent of hydrodynamics any more and only heat conduction problem can be solved in the first approximation to describe the bubble growth. The bubble shape is then determined out of the quasi-static approach that consists to assume that at each time moment bubble has a shape as if it were in equilibrium for the given instantaneous force distribution along its surface. The bubble shape comes from the value of the bubble local curvature $K(l)$ satisfying the modified Laplace equation

$$K\sigma = \lambda + (\rho_L - \rho_V)gy + P_r, \tag{2}$$

where g is the gravity acceleration directed as shown in Fig. 2, y is the ordinate, and λ is the constant along the bubble surface pressure difference between the pressures inside and outside of the bubble. The imposed contact angle θ_{eq} gives a required boundary condition for the shape determination. λ plays a role of the Lagrange multiplier determined knowing the bubble volume V which is defined by the total amount of the latent heat consumed by the growing bubble

$$H\rho_V \frac{\mathrm{d}V}{\mathrm{d}t} = \int q_L(l)\,\mathrm{d}l. \tag{3}$$

The 2D case is assumed hereafter. The only yet undefined quantity in the described problem is $q_L(l)$ is found from the coupled at the heater-liquid interface heat conduction problems in the heater and the liquid (that with moving boundary), both semi-infinite. The vapor is assumed non-conductive and zero heat flux condition is imposed at the dry spot, i.e. at the heater-vapor contact area. The heat is assumed to be generated homogeneously (as by electric current) in the heater volume. The time variation of this volume source is chosen in such a way that the heat flux q_0 at the heater-liquid boundary far from the bubble remains constant in time. The q_0 value will be used as the main control parameter. The constant temperature T_{sat} is given as the boundary condition at the moving bubble interface and also as the initial condition. A small vapor bubble of the radius R_0 is assumed to exist prior to the calculation beginning.

This free boundary problem is solved with the Boundary Element Method (BEM). More details on the solution and on the method can be found in [7].

The evaporation heat flux $q_L(l)$ remains singular at small l in this case, however its divergence is integrable since the exponent α of $q_L(l) \sim l^\alpha$ always falls between -0.5 and -0.8. At the same time $P_r \propto q_l^2$ is non-integrable which leads to a difficulty of the shape determination [1]. To overcome this problem, a cut-off in the flux is needed. From the physics point of view, q_l is bounded by q_{max} [7] due to the limitation on the heat transfer imposed by the maximum molecular speed that introduces a thermal resistance at the bubble interface. Since this cut-off is much larger than the values encountered at the node points used in the numerical calculation, no modification of the isothermal boundary condition is necessary. The same sensitivity of the shape on the P_r integral implies a requirement of the high accuracy of the α determination and thus very fine meshing (of the order of 10^{-4} of the bubble shape) in the contact line vicinity which influences the calculation time. This reason determined our choice of BEM where the node points' number is much less than in any other numerical method: only boundaries between the liquid, vapor and solid domains need to be meshed, not the domains themselves. As a matter of fact, even such fine meshing is not sufficient. To achieve the satisfactory accurate P_r integral calculation, the l^α extrapolation of q_l must be used till q_{max} is reached. The corresponding P_r contribution is integrated analytically and added to the numerically integrated part.

The numerical algorithm has been improved with respect to that used in [7] to get rid of the numerical instabilities which gave rise to temporal oscillations visible e.g. in figure 6 of [7], to be compared with Fig. 3 below. In particular, a new algorithm [11] was used to solve Eq. 2.

Results

The bubble spreading has already been shown in [7] where $\theta_{eq} = 0$ was assumed and no forces tending to remove the bubble from the heater were taken into account. In this paper we introduce the gravity that appears in Eq. 2. To understand the gravity influence, let us first assume that $P_r = 0$ in Eq. 2. The latter has then no solution (i.e. the equilibrium bubble shape) for large V when the contact angle is fixed. A solution of such a truncated problem exist only when V is smaller than some maximum value $V_{max} = V_{max}(\theta_{eq})$ [12], when the capillary adhesion is larger than the Archimedes force. At small θ_{eq}, when V approaches V_{max} during the bubble growth, the dry area size tends to zero and at V_{max} no adhesion to the heater exists any more which means that the bubble departs as a whole.

The account of P_r adds another option due to the P_r^v influence discussed above (Fig. 3). Either the dry spot collapses and the bubble departs as in the $P_r = 0$ case, or its spreading begins. The vapor recoil adhesion then exceeds at once the Archimedes force and keeps increasing with time [8] so that the bubble continues to spread without departing from the heater. This second scenario corresponds to that of the boiling crisis. The lowest value of q_0 at which it occurs (i.e. the transition between the two scenarios) gives the model CHF.

Fig. 3 shows the behavior of the dry spot at a fixed heat flux and a different gravity levels given by the Bond number $\mathrm{Bo} = (\rho_L - \rho_V) g R_0^2/\sigma$. The spreading occurs at $\mathrm{Bo} = 9 \cdot 10^{-5}$

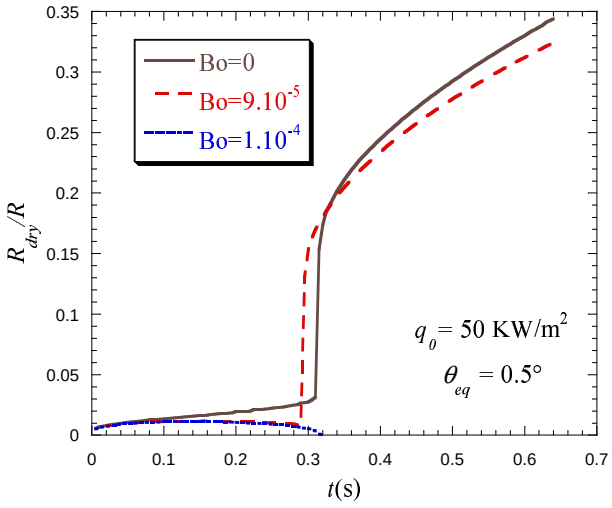


Figure 3. The dry spot evolution with respect to the bubble radius R for fixed heat flux and different gravity levels calculated for the same parameters as in [7] (water at 10 MPa).

(which corresponds to about $0.1g$) while at $\mathrm{Bo} = 10^{-4}$ the bubble departs. It means that the CHF is 50 KW/m^2 for the chosen system parameters.

Note that the insensitivity of the CHF to gravity [4] at low pressures can be explained in the framework of the present model by the influence of the inertial hydrodynamic forces that cause the bubble departure even in the absence of gravity. According to the present model, when the gravity contribution is smaller than that of the inertia, the CHF should be rather defined by the latter than by the former. We will see in the next section that for high pressures, when the bubble growth is slow and the inertial forces are negligible, the CHF is indeed sensitive to the gravity.

EXPERIMENTS AT EXTREMELY HIGH PRESSURE

To overcome the experimental difficulties encountered during the observations of DNB at low pressures, we carry out our experiments at very high pressures, in the vicinity of the critical point defined by the critical pressure p_c and temperature T_c. We take advantage of the so-called "critical slowing down" observed near the critical point. In fact, due to the smallness of the thermal diffusivity, the growing process of a single vapor bubble could be observed during minutes thus allowing for a very detailed analysis. The CHF value is also vanishing at the critical point [9] so that DNB can be examined at a small heat flux that does not necessarily induce a strong fluid motion and high temperature gradients which hinder the optical observations. However, near-critical bubble growth experiments have an important drawback. Since the surface tension becomes very low near the critical point, gravity completely flattens the liquid interface. Reduced gravity conditions are thus necessary to preserve the bubble shape.

In our already performed experiments, the cells are closed and only pure fluid is present in them so that its total mass and volume remains constant. Unlike the conventional boiling experiments, the gas bubble is not nucleated but exists already before the cell heating begins. The bubble growth is then observed.

A particularity of a near-critical fluid consists in the symmetry of its co-existence curve (temperature dependence of ρ_L and

[1] This is easy to understand by recalling the strong dependence of the bubble shape on N given by (1) that involves the P_r integral

ρ_V) with respect to the critical density ρ_c: $(\rho_L + \rho_V)/2 = \rho_c$. When the average density is equal to ρ_c, the vapor volume remains nearly constant and equal to one half of the cell volume throughout the heating. This makes the optical observations even more convenient. The vapor mass however increases (and the liquid mass decreases) during the heating because of the density change.

Two kinds of experiments were carried out up to now. The first studies [5] used SF_6 fluid on board of the Mir space station in the ALICE-2 apparatus designed by the French CNES agency. The choice of SF_6 is made for practical reasons: the critical point of this fluid is $T_c = 45.6°C$, $p_c = 3.8$ MPa and requires much less severe conditions for the experiment than for example water (374°C, 22 MPa). The sequential photos of the growing vapor bubble showed its spreading over the heater. The increase of the apparent contact angle was clearly seen while the actual contact angle was exactly zero (which is a common feature of near-critical fluids).

However, the cells in ALICE-2 were not suitable to control the heat supply or to measure it to obtain the quantitative data. This limitation has been overcome in the experimental H_2 setup that makes use of the magnetic levitation facility [13] at CEA-Grenoble. All further description will concern this data. A cylindrical cell (Fig. 4) of 8 mm diameter and 5 mm height is

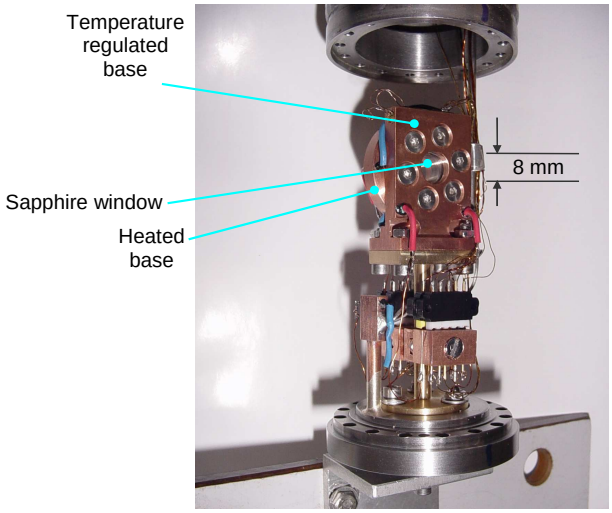


Figure 4. H_2 cell situated inside an "anti-cryostat" under vacuum which is in its turn situated inside another cryostat filled by liquid He to cool the system.

filled with H_2 at critical density. The sapphire windows (cylinder bases) are good heat conductors in the cryogenic temperature range ($T_c = 33$K for H_2). The lateral cell wall is made of stainless steel which is on the contrary the thermal insulator, its heat conductivity being about 1000 times less than that of the sapphire. The copper rings serve to transfer the heat to the windows and to keep the parts of the cell together. The fluid is heated by one of the windows while the temperature of the other is maintained by the temperature regulation system that also permits us to measure the heat flux removed from the cell. The cell can be observed optically through the transparent heater with a light source and a camera. Both are situated outside the cryostat. The optical links are made with the help of light guides.

The gravity is compensated by magnetic forces within 2% in the cell volume. The position of the cell with respect to the magnetic field is chosen so that the residual force positions the bubble against the heating window. In the window plane, the residual force provides the effective gravity directed from the periphery of the window to its center. This force field leads to a curious phase distribution close to the critical point when the surface tension decreases. Most of the more dense liquid phase then masses in the center while the wetting film remains at the cell walls and the windows. As a consequence, the bubble forms a torus (we call this topology annular because of the observed bubble contour). Farther from the critical point, the bubble remains circular as usually.

The heater temperature evolution at DNB is shown in Fig. 5. Before the observation, the heating power is adjusted to com-

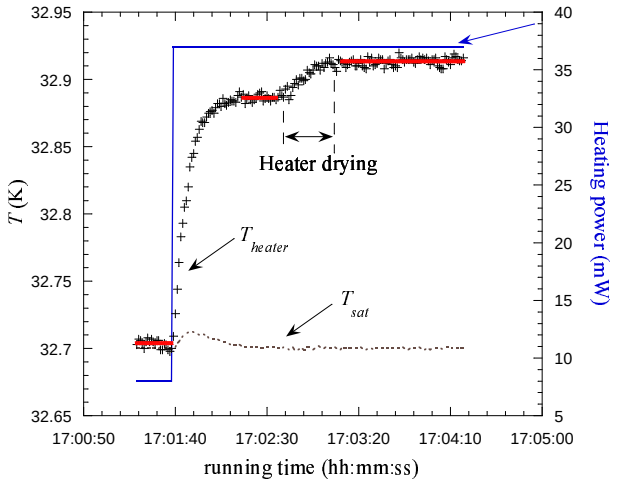


Figure 5. Heater temperature evolution at CHF (crosses). The thick horizontal lines correspond to the averaged values at tree stationary states: at equilibrium, just before and after the DNB. The dotted line reflects the system pressure evolution given by T_{sat}.

pensate for the heat losses and maintained sufficiently long to achieve the thermal equilibration in the isothermal state. When the heat injection starts, small bubbles are nucleated and depart from the heater under the action of residual gravity before coalescing with the large bubble. When the flux approaches the CHF, the dry spot under bubbles nucleates and attains a finite value. At CHF the dry spots under virtually each of the bubbles begin to grow. The larger the dry spot, the faster the growth. At the last stage, the dry spots coalesce and the dryout occurs rapidly. At CHF the complete heater drying (DNB) occurs after a waiting time during which the heater temperature exhibits fluctuations. DNB occurs after the largest of them. The heater is completely dried out and a new stationary conductive state (no convection) is quickly established. In this state, the main part of the heat passes from one base to another by the cell walls. This heat transfer was accounted for by measuring the heat transfer in the empty cell and subtracting the wall flux from the total measured heat flux. The resulting boiling curves are presented in Fig. 6. It shows the dependence of the CHF on very slight changes of the bubble position with respect to the heater. These changes can be induced by slightly displacing the cell with respect to the field so that the wetting film existing at equilibrium between the bubble and the heater, changes its thickness. This sensitivity manifests itself even stronger when the geometry of the large bubble changes from circular to annular. During this

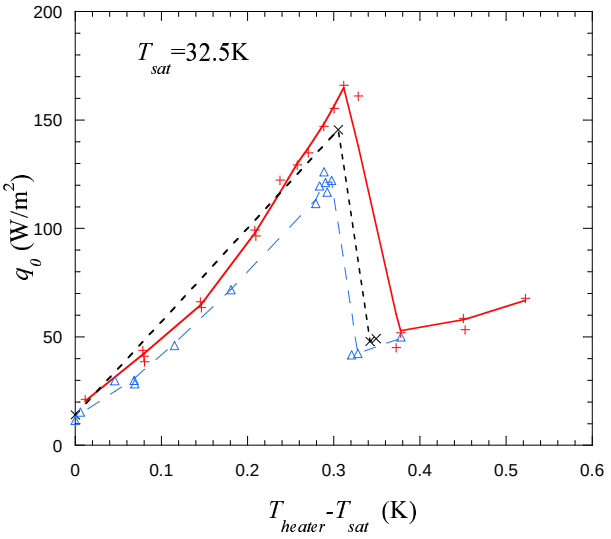


Figure 6. Boiling curves for the same pressure but different effective gravity levels.

change the wetting layer becomes much thicker and occupies smaller portion of the window. The thickness can be judged from the size of the small bubbles that grow inside the layer. After the geometry change occurs, the CHF varies strongly.

This change of bubble position is analogous to the change in the force balance acting on the drop in the usual boiling set-up where there is always a dry spot, at least in a nucleation site area. This dependence can be summarized as follows: the smaller adhesion, the larger is the CHF. This observation is coherent with our vapor recoil model.

Optical observations of the dry spot growth are very interesting. They are especially informative for the annular bubble geometry because the small bubbles are nucleated in the central region of the window, their dynamics can thus be compared to that of the large bubble. For the circular bubble case (farther from the critical point), the small bubbles nucleate and grow only at the periphery of the cell where the liquid layer is thicker. Far from the CHF, the small bubbles first depart from the heater and then coalesce with the large bubble. Their immediate absorption by the large bubble follows. Closer to the CHF, the dry spot under the large bubble forms. The small bubbles also develop a dry spot comparable with their size. Once the dry spot begins to grow, the bubble would not depart as quickly. It would rather continue to grow (in the agreement with our model) until it touches the large bubble and quickly absorbed by it. The growing bubbles in the center slide towards the periphery of the window (probably, because of the larger radial gravity component in the center). The large bubble exhibits the largest rate of the dry spot growth at CHF (Fig. 7).

First, the single dry spot under the large bubble spreads (Fig. 7a), then it coalesces with small bubbles so that their dry spots fuses (Fig. 7b). Ultimately, the whole heater surface dries out during rapid coalescence motions and the fluid becomes very turbid. After the slow relaxation to the transparent state, a stationary conductive state in which the vapor phase covers the heater and the interface forms the hat-like shape (Fig. 7c) where the fluid layer in the center of the window is thicker than at the periphery.

The similar mechanism of the dry spot spreading works also relatively far from the critical point where the bubble is circular. Indeed, the experiments were performed for up to 3% deviation from p_c (which is well beyond the critical region where the anomalous fluctuations define completely the behavior of the fluid).

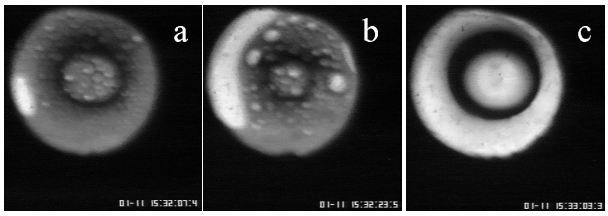


Figure 7. Gas spreading at 32.95K (at annular geometry, the large bubble has a toroidal shape as described in the text) as visualized through the transparent heater in magnetic levitation experiment. (a) Beginning of the dry spot growth. (b) Bubble partially spread. (c) Complete drying of the heater. Nucleated small bubbles are visible in (a-b).

CONCLUSIONS

Basing on the vapor recoil model, the individual bubble spreading is obtained in the simulations. To capture the vapor recoil effect, an extremely delicate analysis of the heat flux maximum in the vicinity of the critical point need to be performed. A threshold exists between the spreading and the bubble departure regimes. This threshold heat flux can be associated with the CHF. This kind of simulation allows to predict the dependence of the threshold on various parameters of the system like contact angle, thermal properties of the heater and the liquid, etc.

The experiments at nearly critical pressure can give very detailed information about the DNB because of the small CHF value and the slowness of the bubble growth. The reduced gravity conditions are however required to observe the bubbles. During the DNB, we observed clearly the growth of individual dry spots under the bubbles prior to their coalescence. This allows us to suggest spreading of individual bubbles as the triggering mechanism for the DNB. This picture agrees with the vapor recoil model suggested earlier.

ACKNOWLEDGMENT

We acknowledge the partial financial support from CNES. We are grateful to V. K. Polevikov for the helpful correspondence.

NOMENCLATURE

Bo Bond number
g gravity acceleration [m^2/s]
H latent heat [J/kg]
K curvature [m^{-1}]
l coordinate varying along the bubble contour
N vapor recoil strength
p pressure [N/m^2]
P_r vapor recoil pressure [N/m^2]
q heat flux [W/m^2]
R bubble radius [m]
t time [s]
T temperature [K]
V 2D-bubble volume [m^2]
y ordinate
α q_L exponent
η rate of evaporation [kg/(s·m^2)]

θ liquid contact angle
λ vapor/liquid pressure difference [N/m^2]
ρ mass density [kg/m^3]
σ surface tension [N/m]
sat saturation
c critical
v vertical
eq equilibrium
ap apparent
0 initial
max maximum
V vapor
L liquid

REFERENCES

[1] N. Zuber, On the stability of boiling heat transfer, *Trans. Am. Soc. Mech. Engrs*, vol. 80, p. 711, 1958.

[2] Yu. A. Buyevich, Towards a Unified Theory of Pool Boiling — the Case of Ideally Smooth Heated Wall, *Int. J. Fluid Mech. Res.*, vol. 26, pp. 189–223, 1999.

[3] V. S. Nikolayev & D. A. Beysens, Boiling crisis and non-equilibrium drying transition, *Europhysics Letters*, vol. 47, pp. 345–351, 1999.

[4] J. Straub, Boiling Heat Transfer and Bubble Dynamics in Microgravity, *Adv. Heat Transfer*, vol. 35, pp. 57–172, 2001.

[5] Y. Garrabos, C. Lecoutre-Chabot, J. Hegseth, V. S. Nikolayev, D. Beysens, & J.-P. Delville, Gas spreading on a heated wall wetted by liquid, *Phys. Rev. E*, vol. 64, 051602, 2001.

[6] M. Barthes, C. Reynard, R. Santini & L. Tadrist, Détermination des caractéristiques géométriques de la croissance d'une bulle de vapeur et des transferts de chaleur associés : influence des incondensables sur le déclenchement d'instabilités convectives, *Mécanique & Industries*, vol. 6, pp. 257–262, 2005.

[7] V. S. Nikolayev, D. A. Beysens, G.-L. Lagier, & J. Hegseth, Growth of a dry spot under a vapor bubble at high heat flux and high pressure, *Int. J. Heat Mass Transfer*, vol. 44, pp. 3499–3511, 2001.

[8] V. S. Nikolayev, D. Beysens, Y. Garrabos, Crise d'ébullition : inhibition du détachement de la bulle de vapeur par la force de recul, *Mécanique & Industries*, vol. 5, pp. 553–558, 2004.

[9] L. S. Tong, *Boiling Heat Transfer and Two-Phase Flow* (2nd Edn.), Taylor & Francis, New York, 1997.

[10] Yu. A. Buyevich, Towards a Unified Theory of Pool Boiling — the Case of Ideally Smooth Heated Wall, *Int. J. Fluid Mech. Res.*, vol. 26, pp. 189–223, 1999.

[11] V. K. Polevikov, Methods for numerical modeling of two-dimensional capillary surfaces, *Computational Methods in Appl. Math.*, vol. 4, pp. 66–93, 2004.

[12] V. S. Nikolayev, D. Beysens, La crise d'ébullition vue comme l'étalement des bulles sur la paroi chauffante, *Proc. 17ème Congrès Français de Mécanique*, Troyes, 29/8-2/09 2005, CD-ROM, 2005.

[13] D. Chatain & V. S. Nikolayev, Using magnetic levitation to produce cryogenic targets for inertial fusion energy: experiment and theory, *Cryogenics*, vol. 42, pp. 253 – 261, 2002.